
This is an electronic reprint of the original article.
This reprint may differ from the original in pagination and typographic detail.

Aleksi, Tamminen; Pälli, Samu Ville; Ala-Laurinaho, Juha; Rexhepi, Sazan; Taylor, Zachary
Ghost imaging at submillimeter waves: correlation and machine learning methods

Published in:
Radar Sensor Technology XXVII

DOI:
[10.1117/12.2663776](https://doi.org/10.1117/12.2663776)

Published: 01/01/2023

Document Version
Publisher's PDF, also known as Version of record

Please cite the original version:
Aleksi, T., Pälli, S. V., Ala-Laurinaho, J., Rexhepi, S., & Taylor, Z. (2023). Ghost imaging at submillimeter waves: correlation and machine learning methods. In *Radar Sensor Technology XXVII* (Vol. 12535). (SPIE Conference Proceedings). SPIE. <https://doi.org/10.1117/12.2663776>

This material is protected by copyright and other intellectual property rights, and duplication or sale of all or part of any of the repository collections is not permitted, except that material may be duplicated by you for your research use or educational purposes in electronic or print form. You must obtain permission for any other use. Electronic or print copies may not be offered, whether for sale or otherwise to anyone who is not an authorised user.

PROCEEDINGS OF SPIE

SPIDigitalLibrary.org/conference-proceedings-of-spie

Ghost imaging at submillimeter waves: correlation and machine learning methods

Aleksi Tamminen, Samu-Ville Pälli, Juha Ala-Laurinaho, Sazan Rexhepi, Zachary Taylor

Aleksi Tamminen, Samu-Ville Pälli, Juha Ala-Laurinaho, Sazan Rexhepi, Zachary Taylor, "Ghost imaging at submillimeter waves: correlation and machine learning methods," Proc. SPIE 12535, Radar Sensor Technology XXVII, 125350S (14 June 2023); doi: 10.1117/12.2663776

SPIE.

Event: SPIE Defense + Commercial Sensing, 2023, Orlando, Florida, United States

Ghost imaging at submillimeter waves: correlation and machine learning methods

Aleksi Tamminen, Samu-Ville Pälli, Juha Ala-Laurinaho, Sazan Rexhepi, Zachary Taylor
Department of Electronics and Nanoengineering, MilliLab, Aalto University, Maarintie 8, 02150
Espoo, Finland

ABSTRACT

We present experimental results on computational submillimeter-wave ghost imaging schemes. The schemes include a dispersive element introducing quasi-incoherent field patterns to the field of view and bucket detection of the back-reflected field across a significantly broad bandwidth. A single bucket detection without discrimination of the field of view into image pixels is used. The imaging experiments at 220-330 GHz with dispersive hologram show successful computational ghost imaging of a corner-cube reflector target at 600-mm distance. Two separate image-forming methods are compared: correlation and machine-learning. In the correlation method, the image is formed by integrating the predetermined quasi-incoherent field patterns weighted with the bucket detections. In the machine-learning method, high image quality can be achieved after non-trivial training campaigns. The great benefit of the correlation method is that, while the quasi-incoherent patterns need to be known, no a priori iterative training to the images is required. The experiments with the correlation method demonstrate resolving of the target at 600-mm distance.

Keywords: Ghost imaging, correlation, machine learning, terahertz imaging

1. INTRODUCTION

Ghost imaging has been proposed as an imaging technique that allows image formation by correlating the quasirandom patterns with the average transmittance or reflectivity with the same quasirandom pattern [1]. Figure 1 shows a sketch of ghost imaging. There, the frequency-diverse field from a dispersive structure is split to reference and bucket receivers. The field in the reference is either experimentally characterized, virtual accurate calculation of the transmitted pattern, or information of the patterns embedded in, e.g., neural network. Ghost imaging has been demonstrated at infrared and visible wavelengths as well as at terahertz frequencies [1],[2],[3]. In this work, we present the first stand-off images using the correlation method and a modified ghost-imaging setup that operates at 220-330 GHz. We also compare the achieved image quality to machine-learning based image reconstruction. The modified ghost imaging setup and the machine-learning method has been described in detail in [4],[5],[6].

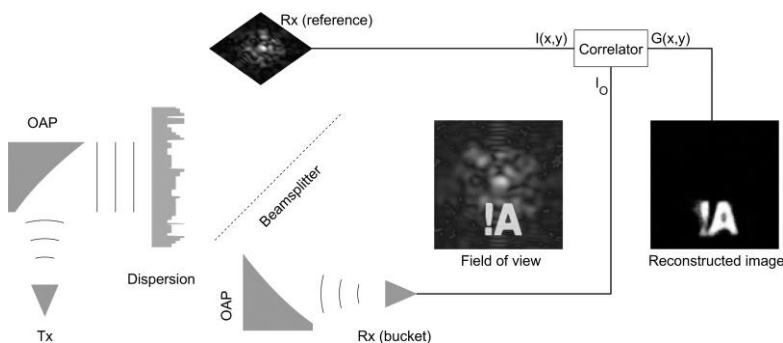


Figure 1. A sketch of ghost imaging setup following the original ghost imaging geometry discussed in [1]. The transmitted waves are dispersed towards target and reference arm. The back reflection from the field of view is detected with a bucket sensor and correlated with the spatial distribution of the dispersed field (in the reference arm).

The dispersion in our work has been introduced with a dielectric hologram, with surface relief structure producing locally varying phase shift in transmission. The quasirandom structure has multiple-wavelength height differences, which results in strong dispersion.

1.1 Correlation method

The significant benefit of ghost imaging is that the reflection from the field of view is sampled only with a stationary bucket receiver that does not carry out spatially discriminating scanning of the target. Instead, the detected fields in reference and bucket arms are correlated as follows:

$$G(x, y) = \frac{1}{N} \sum_{i=1}^N (I_{\text{bucket},i} - \langle I_{\text{bucket}} \rangle) (I_{\text{reference},i}(x, y) - \langle I_{\text{reference}}(x, y) \rangle), \quad (1)$$

where $I_{\text{bucket},i}$ is the i :th intensity measured with the bucket detector and $I_{\text{reference},i}(x, y)$ is either precomputed or measured i :th intensity distribution in the reference arm. The summation in equation is over the N distinctive intensity distributions. The operator $\langle \dots \rangle$ takes average of the quantity over the illumination patterns. Earlier work on optical ghost imaging has considered the SNR of images as function of number of speckles, measurement times, object transmittance contrast. It can be shown that the signal-to-noise ratio in typical ghost imaging is

$$\text{SNR} = \frac{m}{N_{\text{speckle}}} \frac{\Delta T_{\text{min}}^2}{\overline{T^2}}, \quad (2)$$

where m is the number of independent measurements, N_{speckle} is the number of speckle in the beam, ΔT_{min} is the minimum detectable transmittance difference, and $\overline{T^2}$ is the average power transmittance [8]. From (2) it can be seen that the SNR increases linearly with the number of measurements. In typical imaging experiments, m can be from 10^3 to 10^5 .

1.2 Modified ghost imaging setup

Ghost imaging setups used in this work are shown in Figure 2. The imaging experiments involve two separate measurements. First, the highly dispersive field at the target plane is characterized by scanning the receiver in the target plane. Second, the target is scanned in the field of view with simultaneously measured back-reflection from the FoV with the bucket receiver co-located with the transmitter. A 12.7-mm corner-cube reflector was used as the target at 600 mm from the aperture of the dispersive hologram.

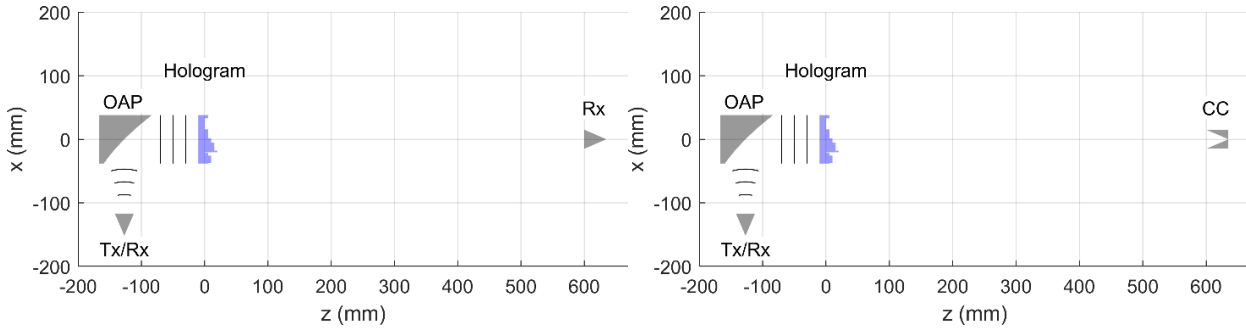


Figure 2. Setup for recording the field (S_{21}) at the target (left) and the back reflection (ρ_{in}) from the corner-cube reflector (right).

The reflection received at the bucket receiver in our method can be described as a two-port model, where the reflection from the quasi-optics (feeding antenna and dispersive element) is combined with the reflection from the FoV:

$$\rho_{\text{in}} = S_{11} + \frac{S_{21}S_{12}\rho_1}{1 - S_{22}\rho_1}, \quad (3)$$

where S_{11} describes the reflection from the quasi-optics and $S_{21} = S_{12}$ describes the propagation between the receiver and the FoV. ρ_1 describes the reflectivity of the target, which is assumed to be negative unity. S_{22} describes the return loss of the target reflectivity to the free space, and it can be assumed to be zero. Time gating can be used to remove the effect of S_{11} from (4). The reflectivity then is

$$\rho_{\text{in}} \approx -S_{21}S_{12} = -S_{21}^2. \quad (4)$$

The correlation in ghost imaging then takes the form:

$$G(x, y) = \frac{1}{N} \sum_{i=1}^N (|\rho_{in,i}| - \langle |\rho_{in,i}| \rangle) (|S_{21,i}(x, y)|^2 - \langle |S_{21,i}(x, y)|^2 \rangle). \quad (5)$$

2. EXPERIMENTS

The ghost imaging measurements were carried out at 220-330 GHz with a setup consisting of a submillimeter-wave extension VNAX WR-3.4 (Virginia Diodes Inc.) connected to network analyzer N5225B PNA (Keysight Technologies). A Pickett-Potter horn (Radiometer Physics GmbH) was used as the feed for an offset parabolic mirror (Edmund Optics) collimating the beam. The hologram transformed the collimated beam into a dispersed in the FoV at 600 mm from the hologram aperture. The back reflection ρ_{in} and S_{21} was measured at 2202 discrete frequencies. The frequency sweep was repeated for all the locations of the corner-cube reflector and S_{21} measurements in the FoV. The FoV extended 100-mm \times 100-mm area with 1-mm increments in x - and y -axis, thus amounting up to 2202×10201 data points. After correlating according to Equation (5), the final image size is 101×101 pixels. The amplitude of the back reflection ρ_{in} and S_{21} are shown in Figure 3. Compared to the reported minimum number of dispersed patterns, $m > 10^3$ (Equation (2)), number of distinctive illumination patterns achieved with this hologram is modest.

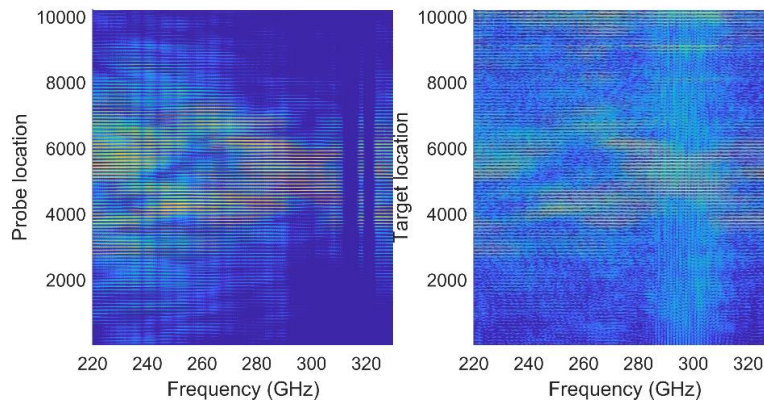


Figure 3. (left) S_{21} -parameter squared, and (right) back reflection ρ_{in} after time gating and subtracting the average value.

3. RESULTS

Images of the targets were calculated according to equation (5). The images were normalized to their maxima and evaluated for the image quality. The images were fitted with elevated Gaussian function:

$$G_{fit}(x, y) = A \exp(-((x - x_0)^2 + (y - y_0)^2)/2\sigma^2) + C, \quad (6)$$

where A is amplitude, x_0 and y_0 are the spot locations in x - and y -axis, σ is the spot width parameter, and C is the constant background level. The width parameter is related to the full width at half maximum (FWHM) as $FWHM = 2\sqrt{2\ln 2}\sigma$. Figure 4 shows images and fitted elevated Gaussian function for successful image recovery close to the optical axis.

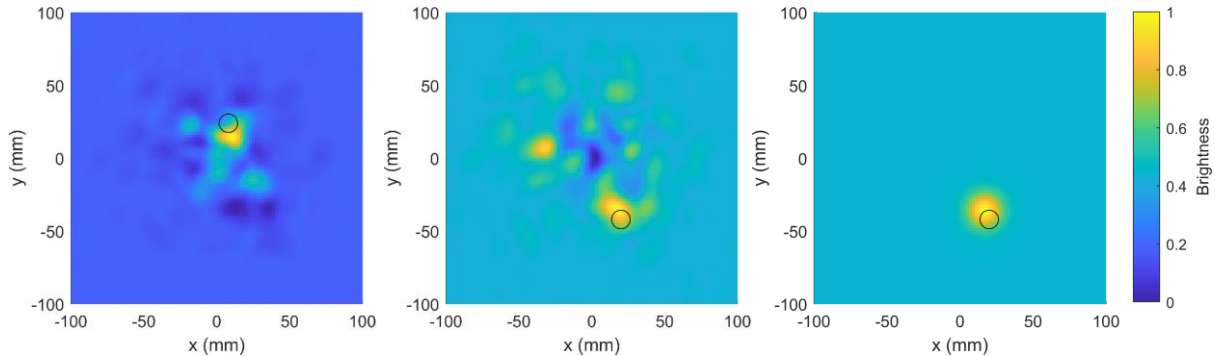


Figure 4. Ghost images when the corner cube is at $x = 8$ mm, $y = 24$ mm (left) and $x = 20$ mm, $y = -42$ mm (center), with an example of fitted elevated Gaussian function (right). The black circles show the location of the corner cube.

The fitted parameters are shown in Figure 5. Before fitting, the ghost images were normalized to their maximum. Close to the center of the FoV, the amplitude in the reconstructed images is close to unity and the FWHM of the spot is approximately less than 20 mm. Further out in the FoV, the amplitude reduces and the FWHM increases. The tapering of the amplitude most probably follows the average amplitude of S_{21} . There is spot location error of 10-20 mm close to the center of the FoV.

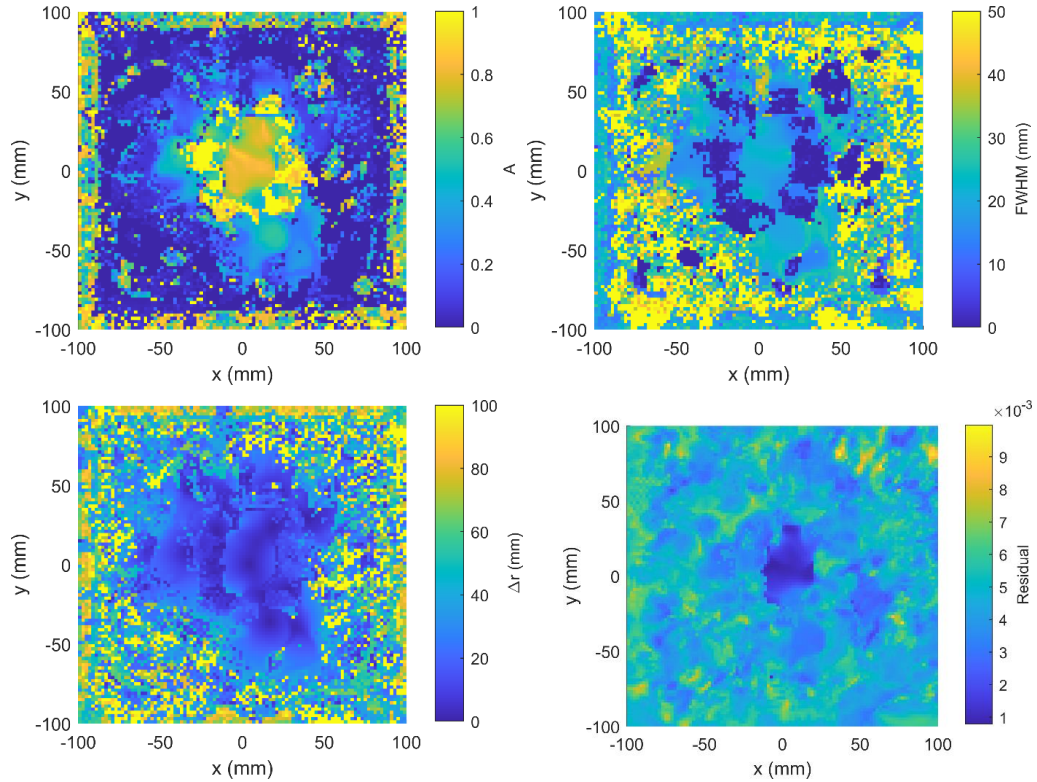


Figure 5. Fitted parameters of the elevated Gaussian function: (top, left) amplitude, (top, right) FWHM, (bottom, left) distance error, and (bottom, right) fit residual. In general, the image reconstruction is most successful within the central 50 mm × 50 mm of the FoV.

In addition to the correlation method, a deep neural network was trained to the images of the corner-cube reflector. The measured back reflection from the corner cube in the 10201 locations was input to the neural network in training. The labels (ground truth images) in the training were augmented disks representing the round corner-cube. The details of the neural network have been reported in [4]. The neural network was trained with 10000 corner-cube locations and the predictions were evaluated at 201 locations. Figure 6 shows the 15th and 30th best image predictions. The image quality is significantly higher compared to the ghost images with the correlation method shown in Figure 4.

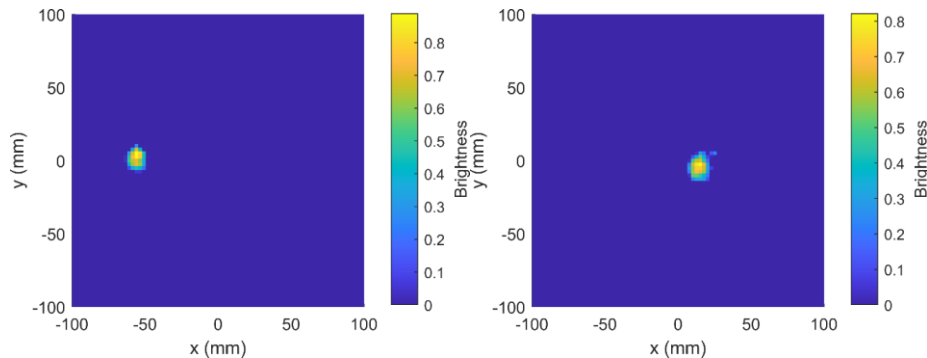


Figure 6. Ghost image results with reconstruction based on neural network: (left) 15th and (right) 30th best image predictions.

4. CONCLUSIONS

We have presented the first results of stand-off ghost imaging at 220-330 GHz. Both correlation as well as neural network were used in the image reconstruction. The imaging experiment was based on the dispersive element, hologram, producing distinct illumination patterns in to the field of view. The patterns were evaluated in the target plane through S_{21} measurements. The reflection from the field of view was recorded with stationary bucket receiver. Our initial experiments with modest number of distinct illumination patterns resulted in successful imaging of a corner-cube target in about half of the examined field-of view with the best image quality resulting in 10-20 mm FWHM at 600 mm distance. The result is promising as it can enable a robust submillimeter-wave imaging technique that relies only on correlation calculation of the bucket reflection with the pre-measured S_{21} . When visually compared to the image reconstruction with a neural network, the image quality with correlation is still lower. However, the correlation method is lightweighted as it does not require tedious iterative pretraining.

REFERENCES

- [1] C. Deng, J. Suo, Y. Wang, Z. Zhang, and Q. Dai, "Single-shot thermal ghost imaging using wavelength-division multiplexing," in *Applied Physics Letters*, vol. 112, no. 5, 051107, 2018.
- [2] L. Olivieri, J. S. Toterogongora, A. Pasquazi, and M. Peccianti, "Time-resolved nonlinear ghost imaging," *ACS Photonics*, vol. 5, no. 8, pp. 3379-3388, 2018.
- [3] L. Olivieri, J. S. Toterogongora, L. Peters, V. Cecconi, A. Cutrona, J. Tunesi, R. Tucker, A. Pasquazi, and M. Peccianti, "Hyperspectral terahertz microscopy via nonlinear ghost imaging," *Optica*, vol. 7, pp. 186-191, 2020.
- [4] A. Tamminen, S.-V. Pälli, J. Ala-Laurinaho, and Z. Taylor, "Millimeter- and submillimeter-wave imaging through dispersive hologram and deep neural networks," in *IEEE Transactions on Microwave Theory and Techniques*, vol. 70, no. 6, pp. 3281-3290, 2022.
- [5] S.-V. Pälli, A. Tamminen, J. Ala-Laurinaho, and Z. Taylor, "Design and characterization of phase holograms for standoff localization at millimeter and submillimeter waves," in *IEEE Transactions on Microwave Theory and Techniques*, vol. 70, no. 1, pp. 907-918, 2022.
- [6] A. Tamminen, S.-V. Pälli, J. Ala-Laurinaho, A. Aspelin, A. Oinaanoja, and Z. Taylor, "Holograms with neural-network backend for submillimeter-wave beamforming applications," in *proceedings of the SPIE PAMMWI XXIII*, 2020, no. 114110C.
- [7] C. Deng, J. Suo, Y. Wang, Z. Zhang, and Q. Dai, "Single-shot thermal ghost imaging using wavelength-division multiplexing," *Applied Physics Letters*, vol. 112, no. 5, article no. 051107, 2018.
- [8] F. Ferri, D. Magatti, L. A. Lugiato, and A. Gatti, "Differential ghost imaging," *Physical Review Letters*, vol. 104, no. 25, article no. 253603, 2010.